A Novel Reactive Element Doping Strategy for Metal Oxides Using Pulsed Laser Deposition: Demonstration with Sulphur in VO_2

Wenqiang Xiang [1,]
https://orcid.org/0000-0001-9683-5253

Baptiste San Nicolas [1, 2, 3]
https://orcid.org/0009-0004-0580-8671

Joëlle Margot [2]
https://orcid.org/0009-0006-3282-0945

Bruno Palpant [3]
https://orcid.org/0000-0003-1376-2533

Mohamed Chaker [1]
https://orcid.org/0000-0001-9781-8842
Mohamed.Chaker@inrs.ca

Abstract

Vanadium dioxide (VO_2) is a phase transition material with significant potential for applications in electrical and optical devices, owing to its remarkable properties such as a sharp change in resistivity and infrared transmittance during the phase transition. Lowering the transition temperature (T_c) while maintaining a high transition amplitude is crucial to many applications; however, conventional doping elements often compromise its transition amplitude. Recent simulations suggest that chalcogen doping, particularly with sulphur, could effectively tune T_c without diminishing the transition performance. Sulphur doping, however, poses challenges due to the tendency of sulphur to react with oxygen during VO_2's high-temperature deposition process, forming volatile sulphur oxides that are lost in the vacuum system. This study introduces a novel sulphur doping approach for VO_2 by using pulsed-laser deposition (PLD) from a V_2S_3 target. By varying the laser repetition rate, sulphur incorporation was precisely controlled without inducing significant defects. Sulphur doping reduced T_c by up to 44.3 °C/at.%, one of the most efficient reductions reported. However, higher sulphur concentrations led to reduced

1 INRS Energy, Materials and Telecommunications Research Centre, Canada.
2 Department of Physics, University of Montreal, Canada.
3 Paris–Saclay University, France.

UNISA university of south africa PRESS
Nano-Horizons
Volume 5 | 2026 | 18 pages
https://doi.org/10.25159/3005-2602/19460
ISSN 3005-2602 (Online)

electrical and optical contrast, attributed to grain boundary strain and disorientation. Lower laser repetition rates facilitated uniform grain growth, sharpening phase transitions and narrowing hysteresis widths. This study underscores the importance of deposition parameters in optimising VO_2 properties and demonstrates the potential of PLD-based strategies for incorporating reactive elements into metal oxides. Future research should further investigate the distinct mechanisms of sulphur doping to refine material properties for advanced applications.

Keywords: vanadium dioxide; pulsed-laser deposition; doping; semiconductor to metal transition; sulphur; thin films

1 Introduction

Vanadium dioxide (VO_2), as a typical phase transition material, has attracted significant attention over the past decades owing to its relatively low phase transition temperature (T_c, ~68 °C) [1]–[6]. When heated above T_c, VO_2 undergoes a structural change from a monoclinic semiconducting phase to a rutile metallic phase [7]. This phase transition is accompanied by a sharp drop in resistivity, typically by 3 to 4 orders of magnitude (OOM), depending on the VO_2 quality [8]. In addition, the infrared transmittance of VO_2 also decreases significantly, by about 50% [9]. Owing to these unique properties, VO_2 has been widely applied in various fields [10]. In particular, VO_2 thin films are extensively used in applications such as electrical switches [4], smart windows [11]–[13], passive radiators [14]–[18], and memory devices [19], owing to their compatibility with diverse electrical and optical devices [20].

In addition to the electrical and optical changes during the phase transition, the transition temperature T_c is also critical to these applications [21]–[23]. Ideally, T_c should be adjustable while maintaining a high electrical and optical contrast [24], [25]. Various methods have been developed to tune T_c in VO_2, including element doping [26], [27], strain engineering [28], [29], oxygen vacancy control [28], electric field stimulation [30], and ion implantation [31], [32]. However, these methods often lead to a reduction in electrical or optical contrast [24], [25]. Among these techniques is element doping, which is the most widely studied and convenient approach [28], [33]. Substitutional electron doping with high-valence elements such as W^{6+}, Mo^{6+}, and Nb^{5+} has been shown to effectively reduce T_c. For example, W doping decreases T_c by approximately 20–28 K/at.% [34]–[40]. Conversely, substitutional hole doping using low-valence elements such as Mg^{2+}, Al^{3+} and Cr^{3+} reduces T_c less effectively and, in some cases, even increases it, depending on the VO_2 synthesis conditions and doping levels [41], [42]. For instance, Mg doping reduces T_c by only 2–3 K/at.% [43], [44], while Cr doping can increase T_c by about 1 K/at.% [45]. Neutral substitutional doping with elements such as Ti^{4+} typically increases T_c by 0.5–4 K/at.% [46], [47], although its impact diminishes at higher doping concentrations, such as 20 at.% [48]. On the other hand, insertional doping with small atoms such as boron has shown the most efficient reduction in T_c, with a decrease of 31.5 K/at.% [49].

A recent study using density functional theory (DFT) simulations systematically explained how element doping modifies T_c of VO_2 while reducing the performance of the phase transition [25]. For example, doping VO_2 with 2.5 at.% W can lower T_c to room temperature because of dopant-induced lattice distortions. However, the electrical contrast drops to less than two OOM because of the additional charge carriers introduced by the W dopants [25], [50]. More recently, sulphur has been identified as a promising dopant for VO_2 owing to its zero net charge transfer with the host material [24], [25]. According to DFT calculations, substituting oxygen with sulphur can reduce T_c by approximately 35 K/at.% without significantly affecting the optical contrast [24], [25]. Experimentally achieving S doping in VO_2 is therefore critical to realising these advantages.

However, sulphur reacts easily with oxygen during the high-temperature deposition process of VO_2 (typically approximately 500 °C [51]), and forms volatile sulphur oxides that are pumped out of the vacuum system. Consequently, it is challenging to dope such an active and gas-producing element in the deposition process of VO_2. Despite these challenges, some success has been achieved with alternative doping approaches. For example, Wan *et al*. [52] successfully doped VO_2 with nitrogen by annealing VO_2 films in an NH_3 atmosphere, but this approach cannot be directly applied to sulphur owing to the safety and toxicity concerns associated with H_2S gas. Another approach, proposed by Chouteau *et al*. [53], used a VN ceramic target and reduced oxygen pressure during PLD to achieve N doping. However, this method introduces additional effects, such as oxygen vacancies, which also influence T_c [54]–[56]. A more effective and direct method to dope VO_2 with elements that are highly reactive with oxygen and produce gaseous byproducts, without introducing additional factors that affect T_c, is therefore highly desirable.

In this study, we propose a novel method for doping oxygen-reactive and gas-producing elements such as sulphur into metal oxides by using PLD. By using a V_2S_3 ceramic target and varying the laser repetition rate from 2 to 10 Hz, we demonstrate that a small amount of sulphur can be incorporated into VO_2 films. To rule out the influence of repetition rate on T_c, both pure and S-doped VO_2 samples deposited at different repetition rates were systematically compared with regard to structure, chemical composition, morphology and phase transition properties. The results show that sulphur doping effectively lowers T_c, but at the cost of a reduction in electrical and optical contrast depending on the doping concentration.

2 Experimental Details

Pure and S-doped VO_2 samples were deposited by using PLD with V and V_2S_3 targets, respectively. A KrF excimer laser (248 nm wavelength) was employed with a fluence of 2 $J \cdot cm^{-2}$ and a spot size of 6 mm^2. Before deposition, the chamber was evacuated to a base pressure of 10^{-6} torr. The substrates used were SiO_2/Si (1 × 1 cm^2), with a SiO_2 layer thickness of approximately 1 μm and a Si substrate thickness of 0.5 mm. During

deposition, the substrate temperature was maintained at 500 °C, and the oxygen pressure was controlled at 15 m torr by a gas flow rate of 5 SCCM. To prepare 150-nm thick pure VO_2 films, three values of laser repetition rate were chosen, namely, 2 Hz, 6 Hz and 10 Hz, yielding samples denoted as V-2 Hz, V-6 Hz and V-10 Hz, respectively. Similarly, S-doped VO_2 samples (VS-2 Hz, VS-6 Hz and VS-10 Hz) were deposited under the same conditions by using V_2S_3 targets.

Deposition rates were determined by conducting test depositions on Si substrates under identical conditions. The film thicknesses were measured using cross-sectional scanning electron microscopy (SEM), and deposition rates were calculated based on the number of laser pulses and the measured thickness. The structural properties of the pure and S-doped VO_2 samples were analysed using grazing-incidence X-ray diffraction (GIXRD). The chemical compositions and valence states were investigated using X-ray photoelectron spectroscopy (XPS) with a Cr Kα radiation source ($h\nu$ = 5414.8 eV) on a PHI Quantes system. The precise sulphur concentration in the doped VO_2 films was measured using Rutherford backscattering spectrometry (RBS). To investigate the effects of S doping on the thin film morphology, SEM images were obtained after depositing a thin gold layer (~a few nanometres) on the samples. The temperature-dependent sheet resistance was measured using a four-point probe station. Reflectance measurements for the pure and S-doped VO_2 films on SiO_2/Si substrates were performed with Fourier transform infrared spectroscopy (FTIR) , as the sample temperature was varied from −5 °C to 100 °C.

3 Results and Discussion

3.1 Structural and Crystallographic Properties

Figure 1 shows the XRD results of the 150 nm pure and S-doped VO_2 samples deposited at various laser repetition rates. The GIXRD spectrum for the pure and S-doped VO_2 samples are displayed in Figure 1(a). All six samples exhibit the typical M1 phase VO_2 pattern (JCPDS 72-0514) [57], with the (011) orientation as the dominant peak. Notably, despite using a V_2S_3 target with a high sulphur content for the deposition of the S-doped samples, no peaks corresponding to V_2S_3 are observed. This indicates that only the M1 phase VO_2 was obtained. This suggests that most of the sulphur was consumed by the oxygen-rich atmosphere during the high-temperature deposition process.

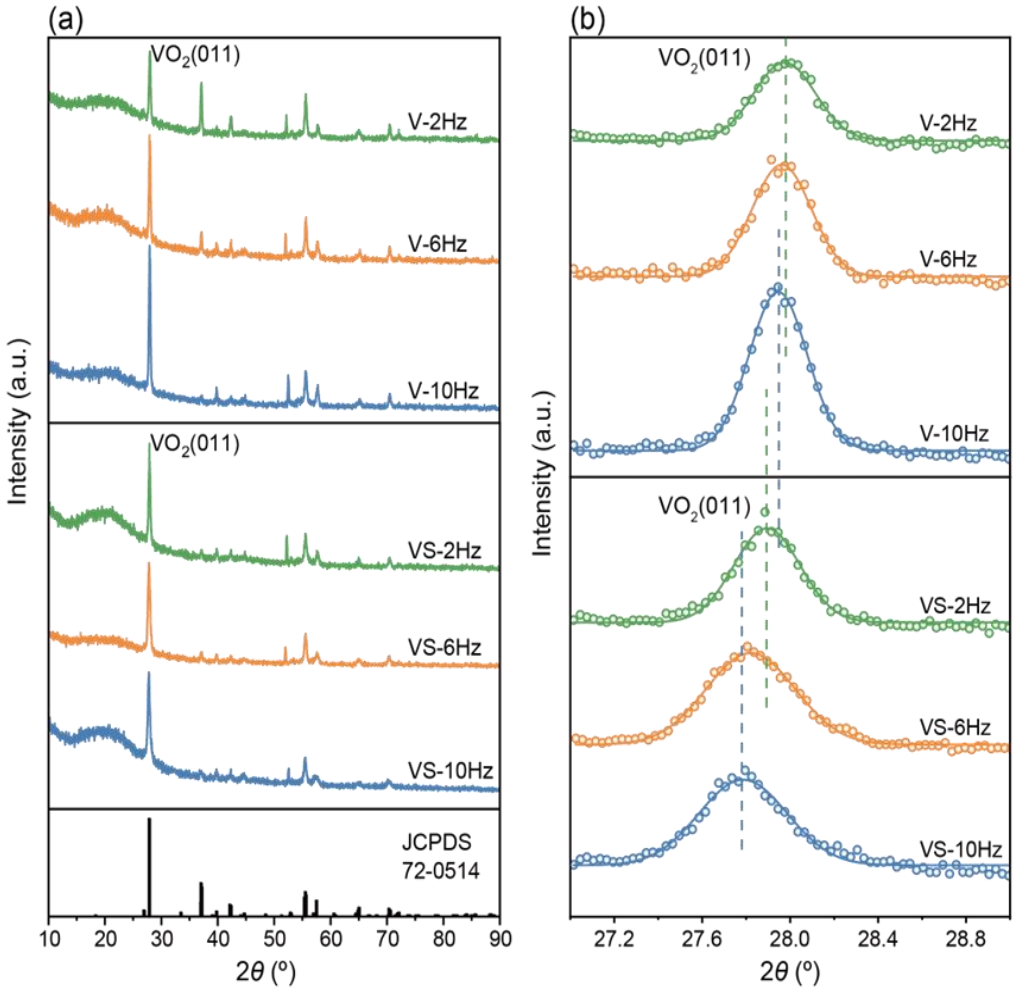

Figure 1: GIXRD spectra of (a) pure and S-doped VO_2 films deposited on SiO_2/Si substrates at laser repetition rates of 2, 6 and 10 Hz, (b) magnified view of the (011) peak for both pure and S-doped VO_2 films, with circles representing experimental XRD data and lines showing Gaussian peak fitting results

The magnified and Gaussian-fitted (011) peak spectra are shown in Figure 1(b). For the pure VO_2 samples, the (011) peak positions remain relatively unchanged, ranging from 27.97° to 27.95° as the laser repetition rate increases from 2 Hz to 10 Hz. However, a slight rightward shift compared to bulk VO_2 at 27.877° is observed, likely due to defects in the thin films, such as grain boundaries and vacancies, which cause local distortions in the lattice structure [58]. This indicates that the laser repetition rate has minimal influence on the lattice parameters of the pure VO_2 samples. Conversely, the (011) peak positions of the S-doped VO_2 samples show more significant variation with increasing

laser repetition rates, shifting from 27.89° to 27.79°. The decrease in the Bragg angle suggests an expansion of the lattice parameters in the S-doped samples [59]. This expansion can be attributed to sulphur atoms (atomic radius ~100 pm) replacing oxygen atoms (~73 pm) in the lattice. Since sulphur is significantly larger than oxygen and still considerably smaller than vanadium (~134 pm), its substitution leads to an increase in the V–S bond length compared to V–O, thereby expanding the lattice. Among the S-doped samples, the VS-10 Hz sample exhibits the largest lattice expansion, likely because higher laser repetition rates allow for more sulphur to be retained in the films, as less sulphur is consumed by the ambient oxygen.

3.2 Chemical Composition and Surface Morphology

The XPS deconvolution results of the V 2p3/2 peak for the pure and S-doped VO_2 samples are shown in Figures 2(a) to 2(c) and 2(d) to 2(f), respectively. All samples exhibit mixed valence states of V^{5+} and V^{4+}, with a significant proportion of V^{4+}, which indicates good stoichiometry of VO_2. The presence of V^{5+} is commonly observed in VO_2 thin films due to surface oxidation in air [60]. In addition, the variation in the V^{5+}/ V^{4+} ratio reflects the oxidation state of the VO_2 film. For example, the V-2 Hz sample exhibits the highest V^{5+} ratio (31%) among the pure VO_2 samples. As the laser repetition rate increases, the V^{5+} ratio decreases, reaching 25% for the V-10 Hz sample.

A similar trend is observed in the S-doped samples: the V^{5+} ratio decreases from 36% for the VS-2 Hz sample to 25% for the VS-10Hz sample. At lower laser repetition rates, the longer interval between pulses can enhance surface diffusion and allow more time for oxidation reactions to occur at the substrate, which contribute to a slightly higher V^{5+} proportion. Interestingly, the S-doped VO_2 samples show a higher V^{5+} ratio at lower repetition rates compared to the pure VO_2 samples. For instance, the V^{5+} ratios for the VS-2 Hz and V-2 Hz samples are 36% and 31%, respectively. This difference becomes less pronounced at 6 Hz and disappears entirely at 10 Hz, where both V-10 Hz and VS-10 Hz samples exhibit identical V^{5+} ratios of 25%. This discrepancy likely arises from the differing doping mechanisms of S at various laser repetition rates. It is possible that lower repetition rates promote substitutional doping with V or O, while higher rates favour interstitial incorporation. This assumption will be further discussed in relation to transition performance and relevant simulation results [24].

To determine the sulphur concentration in the S-doped VO_2 films, RBS analysis was performed on all S-doped VO_2 samples deposited on SiO_2/Si substrates. The stoichiometries of the VS-2 Hz, VS-6 Hz and VS-10 Hz samples were determined to be $V_{0.32}O_{0.6765}S_{0.0025}Ar_{0.001}$, $V_{0.34}O_{0.6545}S_{0.004}Ar_{0.0015}$, and $V_{0.335}O_{0.6585}S_{0.005}Ar_{0.0015}$, respectively. Although it is unclear whether sulphur substitutes vanadium or oxygen, the doping concentration χ was calculated using the formula:

$$\chi = \frac{C_D}{C_V + C_D} \quad (1)$$

where C_D and C_V represent the atomic concentrations of sulphur and vanadium, respectively.

Based on this calculation, the sulphur doping concentrations for the VS-2 Hz, VS-6 Hz and VS-10Hz samples are 0.8, 1.2 and 1.5 at.%, respectively. The argon concentrations in these samples are approximately 0.3, 0.4 and 0.4 at.%, likely originating from contamination in the V_2S_3 target during fabrication. Given argon's inert nature and low concentration (< 0.5 at.%), it is unlikely to affect the transition properties of the VO_2 films. The gradual increase in sulphur concentration from 0.8 to 1.5 at.% with higher laser repetition rates confirms that more sulphur atoms from the V_2S_3 target are incorporated into the VO_2 films during PLD.

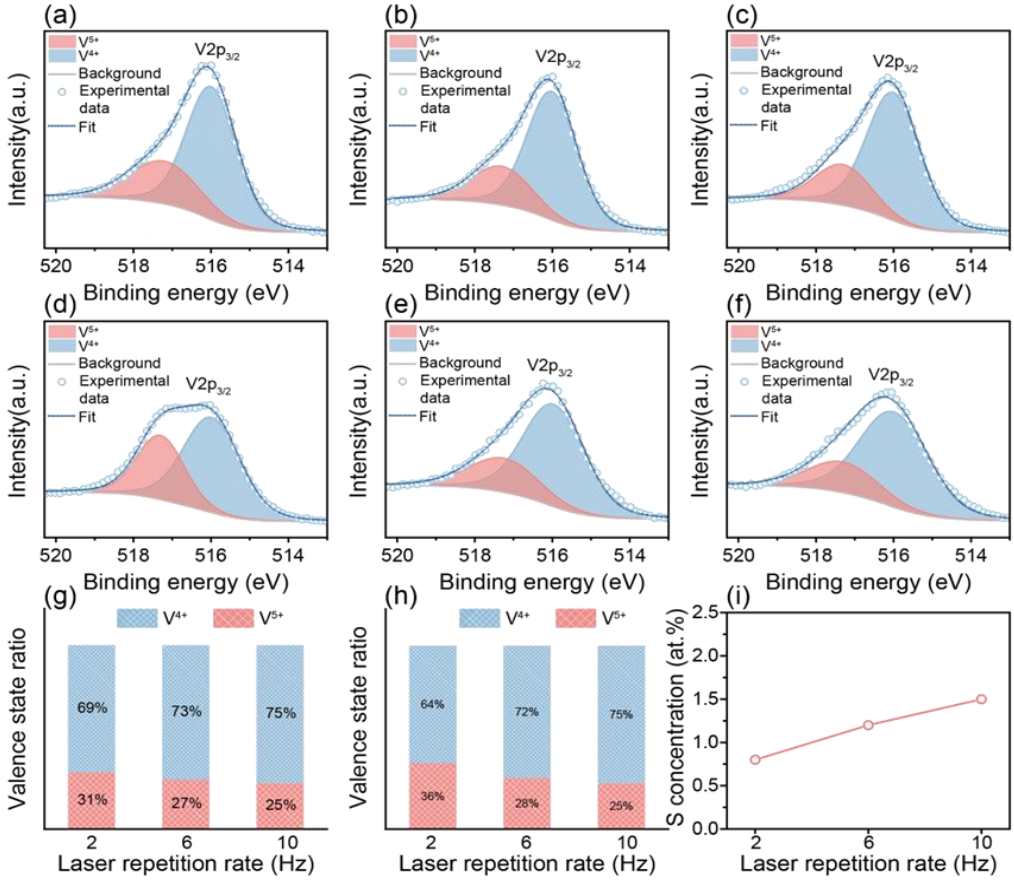

Figure 2: Deconvoluted results of V $2P_{3/2}$ peak of pure VO_2 samples deposited with laser repetition rate of (a) 2, (b) 6, and (c)10 Hz, and S-doped VO_2 samples deposited at (d) 2, (e) 6, and (f) 10 Hz, respectively. The ratio of V valence state (V^{4+} and V^{5+}) in (g) pure VO_2 samples and (h) S-doped VO2 samples deposited with different laser repetition rates. (i) The S concentration in the S-doped samples with respect to the corresponding laser repetition rate determined by Rutherford backscattering spectrometry

The surface morphology of pure and S-doped VO_2 samples prepared at various laser repetition rates is shown in Figure 3, with their respective grain size distributions illustrated in the inset. Among the pure VO_2 samples, the V-2Hz sample exhibits the largest grain size, approximately 94 nm, which gradually decreases to ~82 nm for the V-10 Hz sample. This reduction in average grain size can be attributed to two possible factors. First, at lower repetition rates, the longer interval between laser pulses allows more time for atomic diffusion and rearrangement in the film, facilitating the growth of larger grains. Second, according to the Movchan-Demchishin structural zone model, the growth mechanism for VO_2 is predominantly surface diffusion [61]. XPS analysis reveals that the V-2 Hz sample contains a higher proportion of V^{5+}, which indicates an increased presence of $V_{2n}O_{5n-2}$ Wadsley phases [62]. These phases have lower melting points compared to VO_2, and their dominant growth mechanism is bulk diffusion [63].

Consequently, during the coalescence step, selective orientation becomes more pronounced, driven by a reduction in total grain boundary area and minimisation of surface and interface energies [64]. This results in the formation of larger grains with lower surface and interface energies, as observed in the V-2 Hz sample. In contrast, the impact of repetition rate on grain size is less pronounced for the S-doped samples. For example, the VS-2 Hz (~98 nm) and VS-6 Hz (~97 nm) samples exhibit similar grain sizes. This suggests that sulphur dopants may act as additional nucleation centres during film growth, mitigating the influence of Wadsley phases on the grain size of VO_2. However, a relatively smaller grain size (~82 nm) is also observed for the VS-10 Hz sample, similar to the V-10 Hz sample.

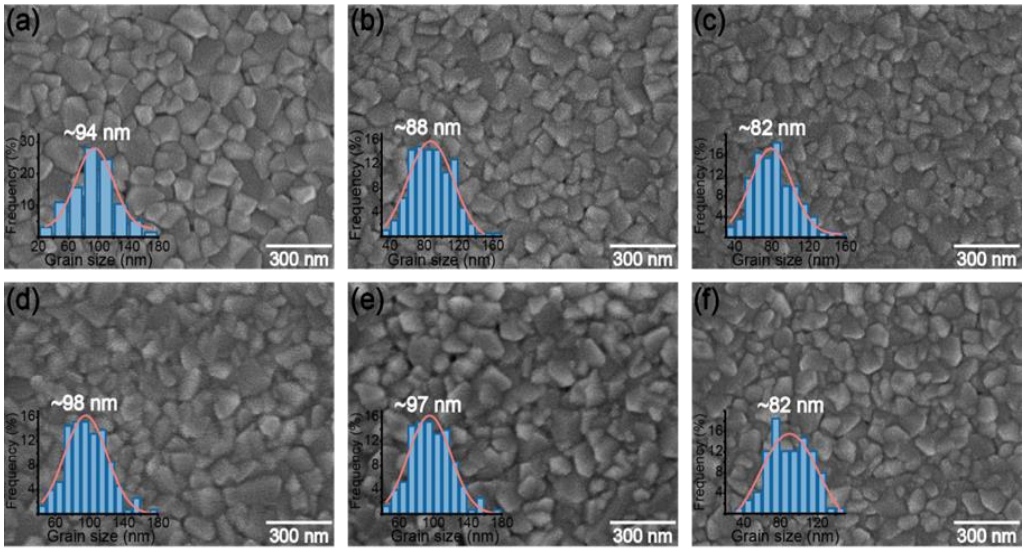

Figure 3: Surface SEM images and grain size distributions of (a) to (c) pure VO_2 samples deposited at laser repetition rates of 2 Hz, 6 Hz and 10 Hz, respectively, and (d) to (f) S-doped VO_2 samples deposited at 2 Hz, 6 Hz and 10 Hz, respectively

3.3 Electrical and Optical Transition Performance

The temperature-dependent sheet resistance of the pure and S-doped VO_2 films is shown in Figures 4(a) and 4(b), and their corresponding transition properties are summarised in Table 1. For the pure VO_2 samples, the transition temperatures (T_{c1}) remain unaffected by variations in laser repetition rates. Interestingly, the electrical contrast (ΔA) exhibits a noticeable improvement as the laser repetition rate decreases. Specifically, as the repetition rate is reduced from 10 Hz to 2 Hz, ΔA increases from 3.1 to 3.6 OOM. This enhancement in electrical transition performance can be attributed to the larger grain size of VO_2 films deposited at lower repetition rates, as observed in the SEM results. Smaller grain sizes result in increased grain boundary density, where the VO_2 films near the grain boundaries are more disoriented and strained [65].

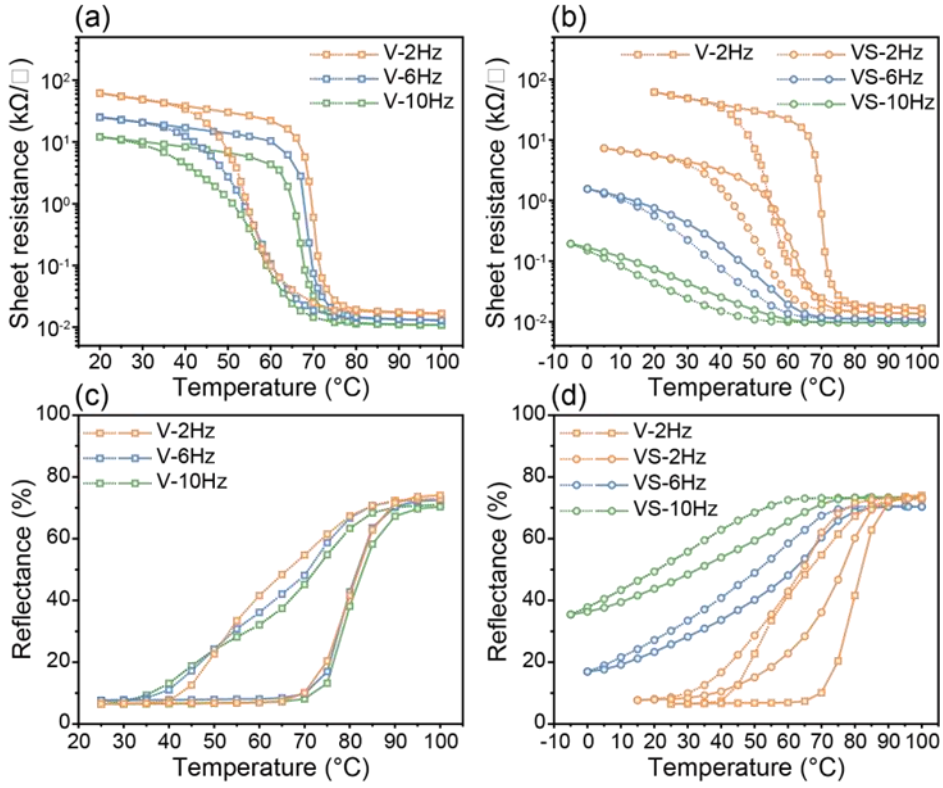

Figure 4: Temperature-dependent sheet resistance results for (a) pure VO_2 samples deposited at laser repetition rates of 2 Hz, 6 Hz and 10 Hz, and (b) a comparison of pure (V-2 Hz) and S-doped VO_2 samples (VS-2 Hz, VS-6 Hz and VS-10 Hz). Temperature-dependent reflectance at 3.4 μm for (c) pure VO_2 samples deposited at 2 Hz, 6 Hz and 10 Hz, and (d) a comparison of pure (V-2 Hz) and S-doped VO_2 samples (VS-2 Hz, VS-6 Hz and VS-10 Hz). Solid lines and dashed lines correspond to heating and cooling branches, respectively

Consequently, the phase transition behaviour of VO_2 in these regions deviates from that of the bulk, leading to a reduction in transition amplitude for films with smaller grains [66]. As shown in Figure 4(b), switching the target material from V to V_2S_3 while maintaining all other deposition parameters results in an 8 °C reduction in T_{c1} for the VS-2 Hz sample compared to the V-2 Hz sample. This reduction in T_{c1} is attributed to S doping, with a concentration determined to be 0.8 at.% via RBS. At higher laser repetition rates, T_{c1} decreases further, from 54 °C to room temperature (23 °C), as increased repetition rates preserve and incorporate more S into the VO_2 films. However, the electrical contrast decreases from 2.7 to 1.3 OOM as the S concentration rises from 0.8 at.% (VS-2 Hz) to 1.5 at.% (VS-10 Hz). Regarding optical properties, the pure VO_2 samples also show an improvement in reflectance change (ΔR) with decreasing laser repetition rates, exhibiting a similar trend to the electrical properties. However, as the S concentration increases from 0.8 at.% to 1.5 at.% for the VS-2 Hz and VS-10 Hz samples, ΔR decreases significantly from 65% to 32%.

Table 1: Electrical and optical transition properties for pure and S-doped VO_2 samples deposited at 2 Hz, 6 Hz and 10 Hz (electrical contrast (ΔA), optical contrast at 3.4 μm (ΔR), order of magnitude (OOM), electrical transition temperature (T_{c1}), optical transition temperature (T_{c2}), electrical hysteresis width (ΔH_1), optical hysteresis width (ΔH_2)

	Electrical transition properties			**Optical transition properties**		
Samples	**ΔA (OOM)**	**T_{c1} (°C)**	**ΔH_1 (°C)**	**ΔR (%)**	**T_{c2} (°C)**	**ΔH_2 (°C)**
V-2 Hz	3.6	62	15	67	69	21
V-6 Hz	3.3	61	13	65	71	18
V-10 Hz	3.1	61	12	64	72	15
VS-2 Hz	2.7	54	10	65	65	13
VS-6 Hz	2.2	38	9	53	48	13
VS-10 Hz	1.3	23	12	38	32	15

The modulation of VO_2 transition behaviour via doping is summarised in Figure 5, which illustrates how different doping levels affect both (a) electrical and (b) optical phase transition properties. Interestingly, the reduction in T_{c1} is not proportional to the increase in S doping concentration. For doping levels below 0.8 at.%, T_{c1} decreases by approximately 10.0 °C/at.%, while at higher doping levels, the reduction is nearly three times greater, reaching ~44.3 °C/at.%. The corresponding reduction rates for the optical transition temperature (T_{c2}) are lower, at ~5.0 °C/at.% for low S doping levels and ~38.5 °C/at.% for higher levels. To the best of our knowledge, the rates of 44.3 °C and 38.5 °C per at.% are among the most efficient reported for lowering the transition temperature of VO_2, surpassing the ~31.5 °C per at.% achieved with boron doping [49].

This two-stage behaviour in the reduction of T_{c1} and T_{c2} may result from a mixed doping mechanism for S in VO_2. For low doping levels (~0.8 at.%), as seen in the VS-2 Hz

sample, the optical contrast remains largely unaffected, with T_{c2} decreasing at ~5 °C/at.%. This aligns with our simulation results for V- or O-substitutional doping previously reported [24], where optical contrast is minimally affected, but the transition temperature is reduced. At higher doping levels, as in the VS-10 Hz sample, the optical contrast decreases to approximately 56% of that of pure VO_2, consistent with simulations of interstitial doping [24]. These simulations predict a reduction of ~75 °C/at.% in transition temperature, with optical contrast reduced to approximately 54% of the value for pure VO_2. Based on the agreement between our experimental results and these simulations, we infer that low-level S doping (~0.8 at.%) is dominated by V- or O-substitutional mechanisms, while interstitial doping becomes predominant at higher concentrations.

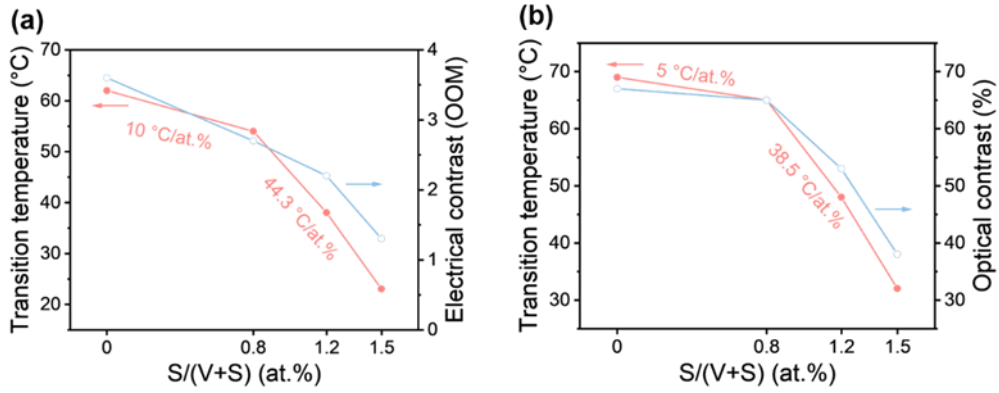

Figure 5: Transition temperature and corresponding phase transition performance of VO_2 at various S doping levels, with regard to (a) electrical and (b) optical properties

In addition to transition temperatures and electrical/optical contrast, the hysteresis width is also crucial to evaluating VO_2 transition performance [67]. As presented in Table 1, the optical hysteresis width ΔH_2 is consistently 3–6 °C wider than the electrical hysteresis width ΔH_1. This can be attributed to percolation effects in the electrical transition, where resistance depends on the percolation threshold of metallic domains, resulting in a sharper transition compared to the gradual optical evolution of mixed-phase domains [68]. Furthermore, the VS-2 Hz and VS-6 Hz samples exhibit narrower hysteresis widths compared to their pure VO_2 counterparts at the same repetition rates for both electrical and optical transitions. This can be explained by the substitution of vanadium or oxygen with sulphur during doping, which slightly increases the grain size by reducing defects or strain at grain boundaries. A similar effect has been observed with low concentrations of Gd doping (~ 1.1 at.%), where the dopants increased the grain size of VO_2 [69]. Conversely, at higher repetition rates, where interstitial doping dominates, the S dopants act as nucleation centres during film growth, resulting in

smaller grain sizes for the VS-10 Hz sample [70]. Consequently, higher hysteresis widths are observed for both electrical and optical transitions, due to increased disorientation and strain near grain boundaries [71].

4 Conclusions

This study presents a novel sulphur doping strategy for VO_2 thin films using PLD with a V_2S_3 target. By varying the laser repetition rate, we achieved controlled sulphur incorporation into VO_2 films, demonstrating the feasibility of doping reactive elements without introducing excessive defects. Structural and compositional analyses confirmed sulphur incorporation, with the observed trends aligning with previous simulation results suggesting substitutional doping at low concentrations and interstitial doping at higher concentrations.

Sulphur doping significantly reduced the phase transition temperature of VO_2, with reductions of up to 44.3 °C/at.% for electrical transitions – among the most efficient reported for VO_2 dopants. However, higher sulphur concentrations led to decreased electrical and optical contrast, attributed to increased grain boundary strain and disorientation. Lower laser repetition rates promoted uniform grain growth, improving phase transition sharpness and narrowing hysteresis widths. These findings emphasise the critical role of deposition conditions in tailoring the phase transition properties of VO_2.

This study underscores the potential of PLD-based doping strategies for VO_2 and other metal oxides to incorporate elements that readily react with oxygen and produce gaseous byproducts during deposition of VO_2 and other metal oxides. Future research should focus on understanding the distinct doping mechanisms at low and high sulphur concentrations to further optimise the material's properties for advanced applications.

5 References

[1] Z. Shao *et al*., "Recent progress in the phase-transition mechanism and modulation of vanadium dioxide materials," *NPG Asia Mater.*, vol. 10, pp. 581–605, Jul. 2018, doi: 10.1038/s41427-018-0061-2.

[2] M. E. Warwick and R. Binions, "Advances in thermochromic vanadium dioxide films," *J. Mater. Chem. A*, vol. 2, no. 10, pp. 3275–3292, 2014, doi: 10.1039/C3TA14124A.

[3] E. E. Chain, "Optical properties of vanadium dioxide and vanadium pentoxide thin films," *Appl. Opt.*, vol. 30, no. 19, pp. 2782–2787, 1991, doi: 10.1364/AO.30.002782.

[4] Y. Ke *et al*., "Vanadium Dioxide: The Multistimuli Responsive Material and Its Applications," *Small*, vol. 14, no. 39, p. 1802025, Sept. 2018, doi: 10.1002/smll.201802025.

[5] A. Zylbersztejn and N. F. Mott, “Metal-insulator transition in vanadium dioxide,” *Phys. Rev. B*, vol. 11, p. 4383, Jun. 1975, doi: 10.1103/PhysRevB.11.4383.

[6] K. Liu *et al*., “Recent progresses on physics and applications of vanadium dioxide,” *Mater. Today*, vol. 21, no. 8, pp. 875–896, Oct. 2018, doi: 10.1016/j.mattod.2018.03.029.

[7] V. R. Morrison *et al*., “A photoinduced metal-like phase of monoclinic VO_2 revealed by ultrafast electron diffraction,” *Sci.*, vol. 346, no. 6208, pp. 445–448, Oct. 2014, doi: 10.1126/science.1253779.

[8] W. Xiang, B. Le Drogoff and M. Chaker, “An innovative method to achieve large-scale high-quality VO_2 thin films: Oxidation of vanadium nitride material deposited by sputtering,” *Appl. Surf. Sci.*, vol. 633, p. 157607, Oct. 2023, doi: 10.1016/j.apsusc.2023.157607.

[9] Y. Yang *et al*., “Transmittance change with thickness for polycrystalline VO_2 films deposited at room temperature,” *J. Alloys Compd.*, vol. 791, pp. 648–654, Jun. 2019, doi: 10.1016/j.jallcom.2019.03.278.

[10] A. Kumar *et al*., “A Comprehensive Review on Synthesis, Phase Transition, and Applications of VO_2, *J. Supercond. Nov. Magn.*, vol. 37, pp. 475–498, Feb. 2024, doi: 10.1007/s10948-024-06705-w.

[11] C. Jiang *et al*., “Phase-change VO_2-based thermochromic smart windows,” *Light Sci. Appl.*, vol. 13p. 255, Sept. 2924, doi: 10.1038/s41377-024-01560-9.

[12] M. Li *et al*., “Hydrothermal Synthesis of VO_2 Polymorphs: Advantages, Challenges and Prospects for the Application of Energy Efficient Smart Windows,” *Small*, vol. 13, no. 36, p. 1701147, Jul. 2017, doi: 10.1002/smll.201701147.

[13] Y. Cui *et al*., “Thermochromic VO_2 for Energy-Efficient Smart Windows,” *Joule*, vol. 2, no. 9, pp. 1707–1746, Sept. 2018, doi: 10.1016/j.joule.2018.06.018.

[14] M. Benkahoul *et al*., “Thermochromic VO_2 film deposited on Al with tunable thermal emissivity for space applications,” *Sol. Energy Mater. Sol. Cells*, vol. 95, pp. 3504–3508, Dec. 2011, doi: 10.1016/j.solmat.2011.08.014.

[15] A. Hendaoui *et al*., “Highly tunable-emittance radiator based on semiconductor-metal transition of VO_2 thin films,” *Appl. Phys. Lett.*, vol. 102, no. 6, Feb. 2013, https://doi.org/10.1063/1.4792277.

[16] A. Hendaoui *et al*., “VO_2-based smart coatings with improved emittance-switching properties for an energy-efficient near room-temperature thermal control of spacecrafts,” *Sol. Energy Mater. Sol. Cells*, vol. 117, pp. 494–498, Oct. 2013, doi: 10.1016/j.solmat.2013.07.023.

[17] B. Xie *et al*., "Enhanced radiative heat transfer and modulation using VO_2-based metasurfaces," *Int. J. Therm. Sci.*, vol. 208, p. 109442, Feb. 2025, doi: 10.1016/j.ijthermalsci.2024.109442.

[18] B. Xie *et al*., "Design of VO_2-based spacecraft smart radiator with low solar absorptance," *Appl. Therm. Eng.*, vol. 236, p. 121751, Jan. 2024, doi: 10.1016/j.applthermaleng.2023.121751.

[19] Y. Zhou and S. Ramanathan, "Mott Memory and Neuromorphic Devices," *Proc. IEEE*, vol. 103, no. 8, pp. 1289–1310, Aug. 2015, doi: 10.1109/JPROC.2015.2431914.

[20] C. Lu *et al*., "Dynamic Manipulation of THz Waves Enabled by Phase-Transition VO_2 Thin Film," *Nanomater.*, vol. 11, no. 1, p. 114, Jan. 2021, doi: 10.3390/nano11010114.

[21] Z. Hiroi, "Structural instability of the rutile compounds and its relevance to the metal–insulator transition of VO_2," *Prog. Solid State Chem.*, vol. 43, nos. 1–2, pp. 47–69, May 2015, doi: 10.1016/j.progsolidstchem.2015.02.001.

[22] D. Wegkamp and J. Stähler, "Ultrafast dynamics during the photoinduced phase transition in VO_2," *Prog. Surf. Sci.*, vol. 90, no. 4, pp. 464–502, Dec. 2015, doi: 10.1016/j.progsurf.2015.10.001.

[23] M. Y. Valakh *et al*., "Variation of the metal-insulator phase transition temperature in VO_2: An overview of some possible implementation methods," *Semicond. Phys. Quantum Electron. Optoelectron.*, vol. 27, no. 2, pp. 136-150, 2024, doi: 10.15407/spqeo27.02.136.

[24] D. Koch and M. Chaker, "Chalcogen Doping as a Promising Strategy to Improve the Thermochromic Properties of Vanadium Dioxide," *J. Phys. Chem. C*, vol. 128, no. 1, pp. 436–444, Jan. 2024, doi: 10.1021/acs.jpcc.3c06079.

[25] D. Koch and M. Chaker, "The Origin of the Thermochromic Property Changes in Doped Vanadium Dioxide," *ACS Appl. Mater. Interfaces*, vol. 14, no. 20, pp. 23928–23943, May 2022, doi: 10.1021/acsami.2c02070.

[26] Y. Wu *et al*., "Decoupling the Lattice Distortion and Charge Doping Effects on the Phase Transition Behavior of VO_2 by Titanium (Ti^{4+}) Doping," *Sci. Rep.*, vol. 5, p. 9328, May 2015, doi: 10.1038/srep09328.

[27] J.-L. Victor *et al*., "Doubling of the Phase Transition Temperature of VO_2 by Fe Doping," *J. Phys. Chem. Lett.*, vol. 12, no. 32, pp. 7792–7796, Aug. 2021, doi: 10.1021/acs.jpclett.1c02179.

[28] M. A. Basyooni *et al*., "Tuning the Metal-Insulator Transition Properties of VO_2 Thin Films with the Synergetic Combination of Oxygen Vacancies, Strain Engineering, and Tungsten Doping," *Nanomater.*, vol. 12, no. 9, p. 1470, Apr. 2022, doi: 10.3390/nano12091470.

[29] S. A. Howard *et al*., "Digital Tuning of the Transition Temperature of Epitaxial VO_2 Thin Films on MgF_2 Substrates by Strain Engineering," *Adv. Mater. Interf.*, vol. 8, no. 9, p. 2001790, May 2021, doi: 10.1002/admi.202001790.

[30] J. Jeong *et al*., "Suppression of Metal-Insulator Transition in VO_2 by Electric Field-Induced Oxygen Vacancy Formation, *Sci.*, vol. 339, no. 6126, pp. 1402–1405, Mar. 2013, doi: 10.1126/science.1230512.

[31] E. M. Heckman *et al*., "Electrical and optical switching properties of ion implanted VO_2 thin films," *Thin Solid Films*, vol. 518, no. 1, pp. 265–268, Nov. 2009, doi: 10.1016/j.tsf.2009.05.063.

[32] P. Jin, S. Nakao and S. Tanemura, "High-energy W ion implantation into VO_2 thin film," *Nucl. Instrum. Methods Phys. Res. B*, vol. 141, nos 1–4, pp. 419–424, May 1998, doi: 10.1016/S0168-583X(98)00177-3.

[33] Y. Xue and S. Yin, "Element doping: a marvelous strategy for pioneering the smart applications of VO_2," *Nanoscale*, vol. 14, no. 13, pp. 11054–11097, 2022, doi: 10.1039/D2NR01864K.

[34] A. Romanyuk *et al*., "Temperature-induced metal-semiconductor transition in W-doped VO_2 films studied by photoelectron spectroscopy," *Sol Energy Mater. Sol. Cells*, vol. 91, no. 19, pp. 1831–1835, Nov. 2007, doi: 10.1016/j.solmat.2007.06.013.

[35] F. Kong *et al*., "Synthesis and thermal stability of W-doped VO_2 nanocrystals," *Mater. Res. Bull.*, vol. 46, no. 11, pp. 2100–2104, Nov. 2011, doi: 10.1016/j.materresbull.2011.06.030.

[36] G. Karaoglan-Bebek *et al*., "Continuous tuning of W-doped VO_2 optical properties for terahertz analog applications," *Appl. Phys. Lett.*, vol. 105, p. 201902, Nov. 2014, doi: 10.1063/1.4902056.

[37] B. Rajeswaran and A. M. Umarji, "Effect of W addition on the electrical switching of VO_2 thin films," *AIP Adv.*, vol. 6, Mar. 2016, doi: 10.1063/1.4944855.

[38] G. Pan *et al*., "Synthesis and thermochromic property studies on W doped VO_2 films fabricated by sol-gel method," *Sci. Rep.*, vol. 7, p. 6132, Jul. 2017, doi: 10.1038/s41598-017-05229-9.

[39] C. Ling *et al*., "W Doping and Voltage Driven Metal-Insulator Transition in VO_2 Nano-Films for Smart Switching Devices," *ACS Appl. Nano Mater.*, vol. 2, no. 10, pp. 6738–6746, Sept. 2019, doi: 10.1021/acsanm.9b01640.

[40] K. Mulchandani *et al*., "Structural transformation and tuning of electronic transitions by W-doping in VO_2 thin films," *Superlattices Microstruct.*, vol. 154, p. 106883, Jun. 2021, doi: 10.1016/j.spmi.2021.106883.

[41] A. O. Suleiman *et al*., "Tuning VO_2 phase stability by a combined effect of Cr doping and oxygen pressure," *Appl. Surf. Sci.*, vol. 571, p. 151267, Jan. 2022, doi: 10.1016/j.apsusc.2021.151267.

[42] M. Zzaman *et al*., "Elevated Transition Temperature of VO_2 Thin Films via Cr Doping: A Combined Electrical Transport and Electronic Structure Study," *J. Electron. Mater.*, vol. 52, pp. 3818–3830, Mar. 2023, doi: 10.1007/s11664-023-10359-0.

[43] N. Mlyuka, G. A. Niklasson and C.-G. Granqvist, "Mg doping of thermochromic VO_2 films enhances the optical transmittance and decreases the metal-insulator transition temperature," *Appl. Phys. Lett.*, vol. 95, Oct. 2009, doi: 10.1063/1.3229949.

[44] J. Zhou *et al*., "Mg-doped VO_2 nanoparticles: hydrothermal synthesis, enhanced visible transmittance and decreased metal-insulator transition temperature," *Phys. Chem. Chem. Phys.*, vol. 15, no. 20, pp. 7505–7511, 2013, doi: 10.1039/c3cp50638j.

[45] B. Brown *et al*., "Electrical and optical characterization of the metal-insulator transition temperature in Cr-doped VO_2 thin films," *J. Appl. Phys.*, vol. 113, May 2013, doi: 10.1063/1.4803551.

[46] B. G. Chae, H. T. Kim and S. J. Yun, "Characteristics of W- and Ti-Doped VO_2 Thin Films Prepared by Sol-Gel Method," *Electrochem. Solid-State Lett.*, vol. 11, p. D53, Apr. 2008, doi: 10.1149/1.2903208.

[47] Y. Hu *et al*., "Preparation and phase transition properties of Ti-doped VO_2 films by sol-gel process," *J. Sol-Gel Sci. Technol.*, vol. 78, pp. 19–25, Jan. 2016, https://doi: 10.1007/s10971-015-3913-z.

[48] I. Takahashi, M. Hibino and T. Kudo, "Thermochromic Properties of Double-Doped VO_2 Thin Films Prepared by a Wet Coating Method Using Polyvanadate-Based Sols Containing W and Mo or W and Ti," *Jpn. J. Appl. Phys.*, vol. 40, p. 1391, 2001, doi: 10.1143/JJAP.40.1391.

[49] T. Hajlaoui *et al*., "Metal-insulator transition temperature of boron-doped VO_2 thin films grown by reactive pulsed laser deposition," *Scripta Materialia*, vol. 177, pp. 32–37, Mar. 2020, doi: 10.1016/j.scriptamat.2019.09.019.

[50] N. Émond, A. Hendaoui and M. Chaker, "Low resistivity $W_xV_{1-x}O_2$-based multilayer structure with high temperature coefficient of resistance for microbolometer applications," *Appl. Phys. Lett.*, vol. 107, Oct. 2015, doi: 10.1063/1.4932954.

[51] W. Xiang *et al*., "High-quality VO_2 films synthesized on polymer substrates using room-temperature pulsed laser deposition and annealing," *Ceram. Int.*, vol. 50, no. 1, pp. 838–846, Jan. 2024, doi: 10.1016/j.ceramint.2023.10.168.

[52] M. Wan *et al*., "Observation of reduced phase transition temperature in N-doped thermochromic film of monoclinic VO_2," *Appl. Surf. Sci.*, vol. 410, pp. 363–372, Jul. 2017, doi: 10.1016/j.apsusc.2017.03.138.

[53] S. Chouteau *et al*., "Investigation of the metal-to-insulator transition of N-doped VO_2(M1) thin films," *Appl. Surf. Sci.*, vol. 554, p. 149661, Jul. 2021, doi: 10.1016/j.apsusc.2021.149661.

[54] Q. Lu *et al*., "Metal-insulator transition tuned by oxygen vacancy migration across TiO_2/VO_2 interface," *Sci. Rep.*, vol. 10, p. 18554, Oct 2020, doi: 10.1038/s41598-020-75695-1.

[55] L. Fan *et al*., "Comprehensive studies of interfacial strain and oxygen vacancy on metal-insulator transition of VO_2 film," *J. Phys.: Condens. Matter*, vol. 28, p. 255002, May 2016, doi: 10.1088/0953-8984/28/25/255002.

[56] K. L. Gurunatha *et al*., "Combined Effect of Temperature Induced Strain and Oxygen Vacancy on Metal-Insulator Transition of VO_2 Colloidal Particles," *Adv. Funct. Mater.*, vol. 30, no. 49, p. 2005311, Dec. 2020, doi: 10.1002/adfm.202005311.

[57] M. Gurvitch *et al*., "VO_2 films with strong semiconductor to metal phase transition prepared by the precursor oxidation process," *J. Appl. Phys.*, vol. 102, Aug. 2007, doi: 10.1063/1.2764245.

[58] C. Chen *et al*., "Influence of defects on structural and electrical properties of VO_2 thin films," *J. Appl. Phys.*, vol. 110, Jul. 2011, doi: 10.1063/1.3609084.

[59] Y. Liu *et al*., "Unraveling Structural Phase Transformation by Simultaneously Determining the Lattice Constants and Mismatch Angle in VO_2/Al_2O_3 Epitaxial Thin Films," *Front. Mater.*, vol. 9, p. 866468, Mar. 2022, doi: 10.3389/fmats.2022.866468.

[60] M. J. Powell *et al*., "Qualitative XANES and XPS Analysis of Substrate Effects in VO_2 Thin Films: A Route to Improving Chemical Vapor Deposition Synthetic Methods?," *J. Phys. Chem. C*, vol. 121, no. 37, pp. 20345–20352, Aug. 2017, doi: 10.1021/acs.jpcc.7b06044.

[61] J. A. Thornton, "High Rate Thick Film Growth," *Ann. Rev. Mater. Sci.*, vol. 7, pp. 239–260, Aug. 1977, doi: 10.1146/annurev.ms.07.080177.001323.

[62] R. Eguchi *et al*., "Angle-resolved photoemission study of the mixed valence oxide V_6O_{13}: Quasi-one-dimensional electronic structure and its change across the metal-insulator transition," *Phys. Rev. B*, vol. 65, p. 205124, May 2002, doi: 10.1103/PhysRevB.65.205124.

[63] Z. Yang, C. Ko and S. Ramanathan, "Oxide Electronics Utilizing Ultrafast Metal-Insulator Transitions," *Ann. Rev. Mater. Res.*, vol. 41, pp. 337–367, Aug. 2011, doi: 10.1146/annurev-matsci-062910-100347.

[64] H. Kim *et al*., "Optimization of the semiconductor-metal transition in VO_2 epitaxial thin films as a function of oxygen growth pressure," *Appl. Phys. Lett.*, vol. 104, Feb. 2014, doi: 10.1063/1.4866806.

[65] F. C. Case, “Modifications in the phase transition properties of predeposited VO_2 films,” *J. Vac. Sci. Technol. A*, vol. 2, pp. 1509–1512., Oct. 1984, doi: 10.1116/1.572462.

[66] J. Jian *et al*., “Roles of grain boundaries on the semiconductor to metal phase transition of VO_2 thin films,” *Appl. Phys. Lett.*, vol. 107, Sept. 2015, doi: 10.1063/1.4930831.

[67] S. Chen *et al*., “Unraveling Mechanism on Reducing Thermal Hysteresis Width of VO_2 by Ti Doping: A Joint Experimental and Theoretical Study,” *J. Phys. Chem. C*, vol. 118, no. 33, pp. 18938–18944, Aug. 2014, doi: 10.1021/jp5056842.

[68] J. F. de Natale, P. Hood and A. B. Harker, “Formation and characterization of grain-oriented VO_2 thin films,” *J. Appl. Phys.*, vol. 66, pp. 5844–5850, Dec. 1989, doi: 10.1063/1.343605.

[69] D. Gu *et al*., “Influence of Gadolinium-doping on the microstructures and phase transition characteristics of VO_2 thin films,” *J. Alloys Comp.*, vol. 705, pp. 64–69, May 2017, doi: 10.1016/j.jallcom.2017.02.138.

[70] T. E. Alivio *et al*., “Postsynthetic Route for Modifying the Metal-Insulator Transition of VO_2 by Interstitial Dopant Incorporation,” *Chem. Mater.*, vol. 29, no. 12, pp. 5401–5412, May 2017, doi: 10.1021/acs.chemmater.7b02029.

[71] R. Lopez *et al*., “Size effects in the structural phase transition of VO_2 nanoparticles,” *Phys. Rev. B*, vol. 65, p. 224113, Jun. 2022, doi: 10.1103/PhysRevB.65.224113.